

# The Sea-Level Changes in Hong Kong From Tide-Gauge Records and Remote Sensing Observations Over the Last Seven Decades

Fang Zou , Robert Tenzer , Hok Sum Fok, Guojie Meng, and Qian Zhao 

**Abstract**—The importance of studying the sea-level change (SLC) in Hong Kong (HK) is emphasized by factors related to high population density, intensive urban, and industrial development, particularly along the coast that involves a considerable land reclamation. To address this issue, we investigate the spatiotemporal characteristics of SLC in the HK territories by analyzing tide-gauge (TG) records collected from 1954 to 2019 and satellite-altimetry (SA) data from 1993 to 2019. The application of the ocean-tide and inverted barometer corrections to TG data substantially decreased uncertainty by achieving a submillimeter accuracy. The SLC rates detected at six TG stations vary significantly even within this relatively small coastline. According to our estimates, the annual rates vary between  $0.32 \pm 0.51$  and  $4.19 \pm 0.46$  mm/yr from 1997 to 2019. These large differences are related to different patterns of ocean currents and the freshwater discharge in the Pearl River Estuary. The empirical orthogonal function analysis confirms the expected increasing rising in SLC with two anomalous periods during 2002–2003 and 2015–2016 that are likely attributed to the El Niño-Southern Oscillation (ENSO). SLCs are positively correlated with the ENSO index and ENSO precedes several months (normally 5 months) the interannual SLC. The analysis of the GPS trends reveals a prevailing subsidence in the HK territories, which aggravates the relative SLC estimates. Between 1997 and 2019, the absolute sea level raised at the annual rate of  $3.17 \pm 1.56$  mm/yr (when using the GPS+TG) and  $2.88 \pm 0.59$  mm/yr (when using SA observations).

**Index Terms**—El Niño-Southern Oscillation (ENSO), land subsidence, satellite-altimetry (SA) observations, sea-level changes (SLCs), tide-gauge (TG) record.

Manuscript received January 8, 2021; revised March 30, 2021 and May 21, 2021; accepted May 24, 2021. Date of publication June 8, 2021; date of current version July 14, 2021. This work was supported in part by the National Key R&D Program of China under Grant 2018YFC1503503, in part by the National Natural Science Foundation of China under Grant 41974012, in part by Hong Kong Research Grants Council under Project 1-ZE8F: “The Assessment of Sea Level Change in Hong Kong,” and in part by the special fund of China Seismic Earthquake Site under Grant 2018CSES0207. (Corresponding author: Robert Tenzer.)

Fang Zou is with the Key Laboratory of Earthquake Forecasting, Institute of Earthquake Forecasting, China Earthquake Administration, Beijing 100036, China, and also with the Department of Land Surveying and Geo-Informatics, Hong Kong Polytechnic University, Hong Kong (e-mail: fangz070720@gmail.com).

Robert Tenzer is with the Department of Land Surveying and Geo-Informatics, Hong Kong Polytechnic University Hong Kong (e-mail: robert.tenzer@polyu.edu.hk).

Hok Sum Fok is with the School of Geodesy and Geomatics, Wuhan University, Wuhan 430079, China (e-mail: xshhuo@sgg.whu.edu.cn).

Guojie Meng and Qian Zhao are with the Key Laboratory of Earthquake Forecasting, Institute of Earthquake Forecasting, China Earthquake Administration, Beijing 100036, China (e-mail: mgj@ief.ac.cn; qianzhao411@126.com).

Digital Object Identifier 10.1109/JSTARS.2021.3087263

## 1. INTRODUCTION

SINCE the 20th century, the global sea level has risen by 10–20 cm [1], [2], which is a slow natural disaster caused by global warming [3], [4], melting of polar glaciers [5]–[9], and the thermal expansion of the upper seawater [10]–[12]. The Intergovernmental Panel on Climate Change projected an indicative range of 26–77 cm global mean sea-level rise (relative rates 1986–2005) by 2100 for 1.5 °C of global warming. This will cause a series of problems, such as coastal wetlands and lowland inundation [13], [14], coastal erosion [15], [16], flood and storm surge disasters [17], [18], and seawater intrusion [19]. A serious impact is particularly expected for economically developed and densely populated coastal areas. Early studies on sea-level change (SLC) mainly focused on the global mean SLCs [8], [10], [20]–[22]. However, the SLC varies differently from one region to another due to two major factors. First, factors, such as high and low tide, storms, and a high atmospheric pressure, make the regional sea surface unable to return to calm. Second, the seabed topography also determines the unevenness of the sea surface. The impact of sea-level rise is especially sensitive along coastal lowlands with a high-density population. Coastal sea-level rises are expected to be much greater than the global mean sea-level rise [23], [24]. It is, therefore, necessary to study the SLC in such regions.

The Hong Kong (HK) territories, situated in South China and close to the east of the Pearl River Estuary on the northern coast of the South China Sea (SCS), have the area of about 1100 km<sup>2</sup> with a population of about 7.5 million, thus being one of the regions with the highest population density in the world. The sea-level rise in this densely populated and low-lying metropolis represents a serious risk to the economic development and human lives because over 60% of the population in HK is concentrated along areas gained from a coastal land reclamation. For these residents, every few centimeters of sea-level increase will bring hidden dangers [25]–[27]. Due to the unique characteristics of bottom topography and the potential impacts of sea-level rise in HK, monitoring of the sea level and understanding of SLCs become especially important.

The long-term tide-gauge (TG) records provide the only means to directly measure a relative SLC over the 20th century [28]. These records are often used to study the SLCs affected by processes, which perturb the positions of the land and sea surface. These processes include the glacial isostatic adjustment,

earthquakes, sedimentation, volume changes in glaciers, and oceanic thermal expansion. Since the 1950s, a number of automatic TGs were installed in HK, currently providing information about a relative SLC for more than 60 years [29], [30]. The TG stations measure a local relative sea level, thus being affected by the absolute SLCs and the vertical land motion. Conversely, the vertical land motion rates from GPS data together with the relative SLC rates from TG stations have been used to estimate the absolute SLCs. The use of GPS data is important, as a considerable subsidence has been observed at some locations in HK [31]–[33]. Since the 1980s, the satellite-altimetry (SA) measurements have been used to estimate the absolute SLC globally. Naturally, both methods can be used for this purpose, even if the use of altimetry data close to the coast is partially restricted by a lower accuracy. We use these approaches to estimate the absolute SLCs in HK based on the analysis of TG, GPS, and altimetry data.

The sea level in HK has been rising at a significant rate in recent decades [25], [29], [34], [35]. Ding *et al.* [30] reported the rising rates of  $2.2 \pm 0.2$  mm/yr in Macau and HK over the latter half-century from the analysis of TG records [30]. Wong *et al.* [36] estimated the sea-level rise at the annual rate of  $7.6 \pm 3.8$  mm in the Quarry Bay (QUB) and  $3.4 \pm 3.1$  mm in the Tai Po Kou (TPK) based on processing the TG data between 1993 and 2003 [36]. During the period from 1954 to 2009, the mean sea level in the Victoria Harbour risen at an average rate of about 2.6 mm/yr [37]. Zhibo *et al.* [35] used the Topex/Poseidon altimetry data and the TG records between 1994 and 2000 to analyze the SLC along the coast of HK. According to their estimates, the relative rate of sea-level rise is 12.18 mm/yr from the TG data, while 7.73 mm/yr from the Topex/Poseidon altimetry data [35]. He *et al.* (2014) used the TG and altimetry data to reconstruct the sea-level trend in the Pearl River Delta over the period between 1959 and 2011. They reported a relative increase at the rate of 4.1 mm/yr over that period. Qu *et al.* [23] reported an increasing trend at the rate of 2–2.7 mm/yr from three TG records in HK and 3.5 mm/yr from altimetry data during 1993–2018 [23].

In HK, the SLC is highly correlated with the El Niño–Southern Oscillation (ENSO) [30], [31], [36], [37]. Ho *et al.* (2000b) successfully identified the third empirical orthogonal function (EOF) mode of sea level (explaining 10% of the variance) that is related to the ENSO [38]. Wu and Chang [39] illustrated strong interannual variations in the SCS that are highly correlated with the ENSO events [39]. Cheng *et al.* (2014) found surface wind anomalies associated with ENSO and explained the sea-level anomaly pattern in the interior SCS [40]. A secular sea-level trend of  $6.7 \pm 2.7$  mm/yr was found to be much higher than the corresponding global rate, and the interannual sea-level variation to be correlated with the Niño 3.4 index [41]–[43]. In the above-mentioned studies, TG records were rarely used to analyze the regional SLCs and the relationship between the regional SLCs (rather than just using one TG station) and the ENSO.

In this study, we applied the EOFs method to analyze monthly sea-level records collected at six TG stations to estimate the regional SLCs in HK and then inspected a potential role of the ENSO events in these changes. This method is a mathematical

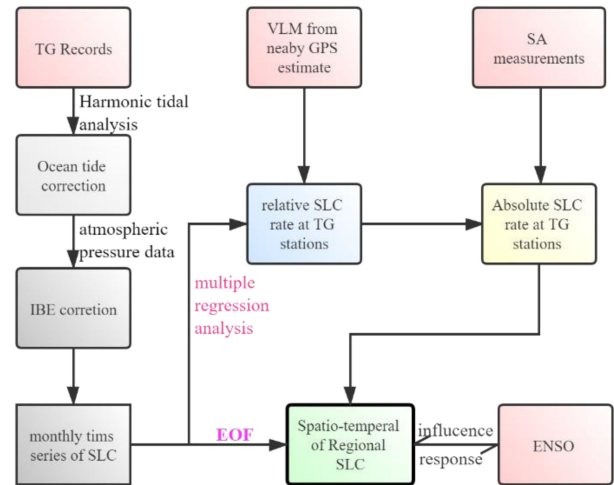


Fig. 1. Flowchart of the study.

dimensionality reduction method, which can reflect the main characteristics of SLCs on the spatial scale. As a common technique for data analysis, the EOF method can analyze and excavate the change law of long time series of sea level and then analyze the causes of SLCs. The advantage of this method is that a typical field is determined by the characteristics of time series of variables, instead of being determined artificially in advance, so it can better reflect the basic structure of the field. It can decompose the irregular distributed sites in a limited area and the decomposed spatial structure has a clear physical meaning. Compared with a simple regional average, the principal component (PC) decomposition can better extract the consistent changes of sea level in the study area. For this purpose, we used the six TG records between 1954 and 2019 to estimate the relative SLCs. Although the ocean-tide and atmospheric pressure effects have been taken into consideration in published studies of the long-term SLCs in HK, the specific magnitudes of these effects are rarely mentioned. We, therefore, first quantified the magnitudes of both effects on SLCs.

Finally, we analyzed a possible link between the interannual SLCs and global climatic events. For a more comprehensive analysis of the absolute and relative SLCs in HK, we also estimated the absolute SLC rates from the analysis of TG and GPS data and compared the results with the SA estimates. The article is organized into five sections and the flowchart of this study was shown in Fig. 1. The input data acquisition is described in Section II. Processing strategies are explained in Section III. The results are presented and discussed in Sections IV and V, respectively. Finally, Section V concludes the article.

## II. DATA

### A. TG Data

The HK real-time tide information service provides the real-time tidal data from 14 TG stations, some of them recorded over a century. Currently, there are 11 TG stations in HK. The Chek Lap Kok station is managed by the Airport Authority. The Ko

TABLE I  
STATISTICS OF TG STATIONS IN HK

Station Name	Latitude and Longitude	Operation Period
North Point/ Quarry Bay	22°18'N 114°12'E/ 22°17'N 114°13'E	1954-1985/ 1986-2020
Shek Pik	22°13'N 113°54'E	1997-2020
Tai Miu Wan	22°16'N 114°17'E	1994-2020
Tai Po Kau	22°27'N 114°11'E	1963-2020
Tsim Bei Tsui	22°29'N 114°01'E	1974-2020
Waglan Island	22°11'N 114°18'E	1976-2018

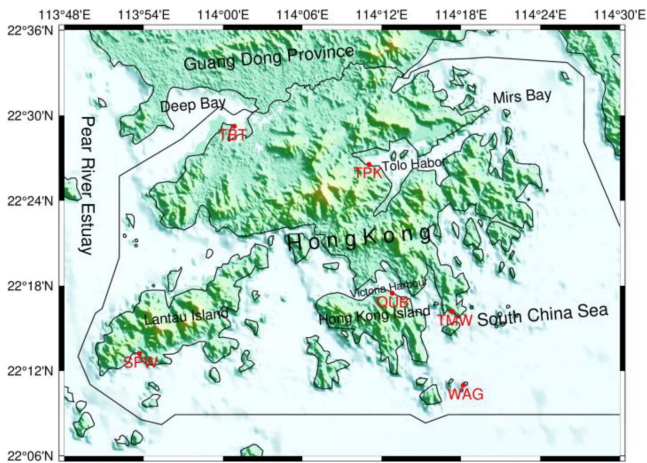


Fig. 2. Spatial distribution of TG stations in HK used in this study.

Lau Wan, Kwai Chung, Ma Wan, and Cheung Chau stations are managed by the Hydrographic Office of the Marine Department. The QUB, Tsim Bei Tsui (TBT), Waglan Island (WAG), TPK, Shek Pik (SPW), and Tai Miu Wan (TMW) stations are managed by the HK Observatory.

Since records from TG stations managed by the Hydrographic Office of the Marine Department and the Airport Authority are not publicly available, we used only the TG data from six stations managed by the HK Observatory, specifically QUB, SPW, TMW, TBT, TPK, and WAG. Their statistical information is summarized in Table I, and their location is shown in Fig. 2. The North Point station provided 32 years (1954–1986) of hourly data, thus being the longest operational TG station in HK. This station was subsequently moved to an adjacent location in the QUB that has been in operation since the beginning of 1986. The TG data for the QUB used in this study, thus, represent two datasets obtained at two different locations in the QUB (22°18' N, 114°13' E) and the North Point (22°18' N, 114°12' E). Both sites are located in areas of reclaimed land but were geodetically connected. We note that the TG station (and related facilities) in the WAG was devastated during the Typhoon Mangkhut in 2018. The heights of all TG stations are defined in the Chart Datum (CD), which is 0.146 m below the HK Principal Datum (HKPD) (about 0.88 m below the Yellow Sea Datum). The CD is used by the royal observatory for all sea-level observations, and the

HKPD is adopted by the Crown Lands and Survey Office of the HK Government for the design of all civil engineering works.

The eastern side of HK is open to the influences of the coastal cold current that carries colder waters from the East China Sea along the Taiwan Strait to the south China coast in winter and the Kuro Shio current that transports warm waters from the Pacific across the Luzon Strait into the SCS in springtime. During the summer months, the Hainan current that carries warm waters up to the northeastern coast of the SCS prevails. The western side of HK territories is bordering with the Pearl River Estuary. The freshwater discharge via the Pearl River Estuary and sedimentation distribution at the estuary exert influence on the HK waters. This influence declines from west to east [29], [37]. The QUB, TPK, TMW, and WAG stations are located on the eastern side of HK, while the TPT and SPW stations are close to the Pearl River Estuary.

The raw TG datasets from the HK Observatory are contaminated by unexpected anomalies, such as outliers, offsets, and gaps. In the data preprocessing stage, we removed outliers based on applying a variance threshold technique. We further implemented a noise assessment algorithm to find possible offsets periods and to eliminate their corresponding observations from time series. We then used a least squares analysis to fill the gaps in the time series. As an example, the raw and processed time series of the TG record taken at the QUB station is shown in Fig. 3. Many outliers and offsets are obvious in raw data [see Fig. 3(a)]. The time series after removing outliers is shown in Fig. 3(b). The daily mean sea-level estimates, as shown in Fig. 3(c), were obtained by a simple averaging of the hourly data. The monthly mean sea-level data, as shown in Fig. 3(d), were then obtained by applying a similar procedure to the daily averaged data.

## B. SA data

We used the Ssalto/Duacs monthly mean and climatology-gridded sea-level anomalies. The products from all available SA missions, which include Jason-1/2/3, Sentinel-3A, HY-2A, Saral/AltiKa, Cryosat-2, ENVISAT, GFO, ERS1/2, and TOPEX, are distributed by the archiving, validation, and interpretation of satellite oceanographic (AVISO) data ([www.aviso.oceanobs.com](http://www.aviso.oceanobs.com)). The monthly near-global sea-level anomaly data are provided on a  $0.25^\circ \times 0.25^\circ$  grid between 1993 and 2020. The authors of these datasets applied the GOT4.8 global ocean-tide model and dynamic atmospheric correction to remove the effects of the ocean tides and atmospheric pressure (i.e., the inverted barometer correction).

## C. GPS Data

We used the GPS time-series solutions provided by the Nevada Geodetic Laboratory (NGL). These solutions are prepared by using the precise point positioning data analysis strategy from Système d'Observation du Niveau des Eaux Littorales (SONEL) in the global sea-level observing system (GLOSS). The GipsyX software (version 1.0) from the Jet Propulsion Laboratory was employed to produce daily position time series for over 17 000 globally distributed stations. The NGL is aligned

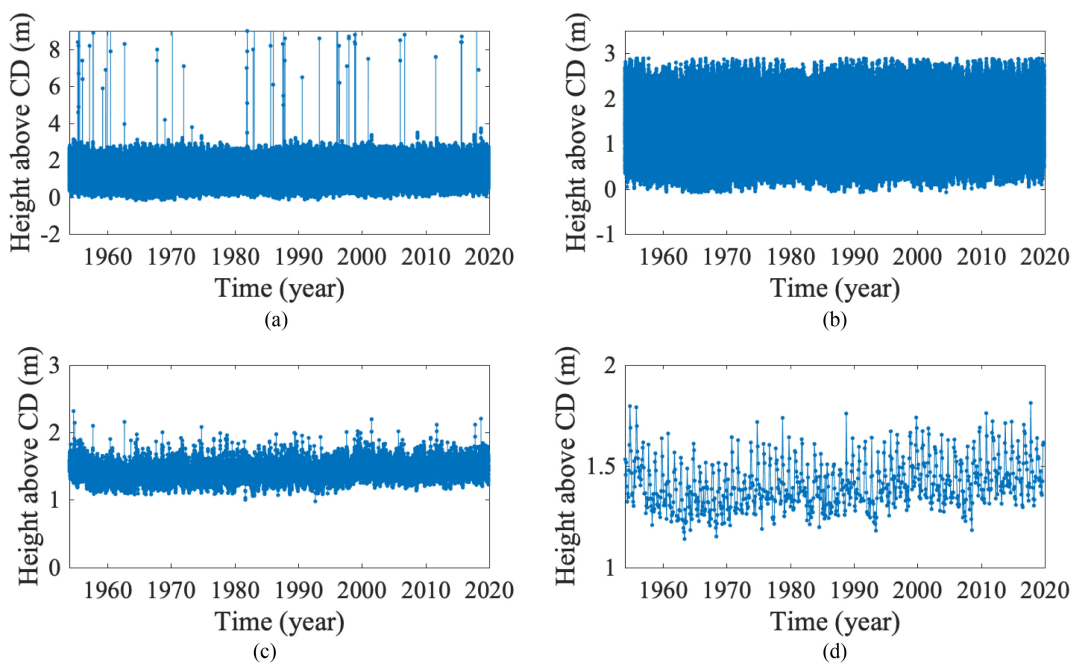


Fig. 3. TG data from the QUB station. (a) Raw data. (b) Preprocessed. (c) Daily averaged. (d) Monthly averaged.

in the IGS14 reference frame. Among more than 17 000 stations processed by NGL, as many as 1014 have actually been identified as colocated or nearby TGs. The GPS trends of 904 stations have been produced by NGL using the MIDAS estimator. The GPS stations with long-term records were selected to be located as close as possible to TGs ( $<10$  km), so ten GPS stations are chosen as colocated or nearby GPS stations, including five stations in Kowloon and the New Territories (HKSL, HKKT, HKSC, HKST, and HKWS), three stations in the Lantau Island (HKCL, HKNP, and HKMW), and two stations in the HK Island (HKQT and HKOH).

#### D. Sea-Level Atmospheric Pressure Data

The atmospheric pressure changes cause sea-level fluctuations [44]. Generally, when the air pressure is high, the sea level is low, and vice-versa. SLCs caused by changes in air pressure are collectively called the inverted barometer effect. When the air pressure rises by 1 mbar, the sea surface height drops by about 1.01 cm [45]. Since SA data products are corrected for this effect, we corrected only TG records. For this purpose, we applied the inverse barometer pressure correction to the TG data by using the sea-level surface pressure obtained from the National Centers for Environmental Prediction (NCEP) (<http://www.cdc.noaa.gov>). This agency provides the sea surface air pressure data on a  $2.5^\circ \times 2.5^\circ$  global grid from 1948 with a time-sampling interval of 6 h as well as daily and monthly averages.

#### E. ENSO Index

The ENSO refers to both the El Niño and La Niña phenomena. The ENSO is an irregular interaction between the atmosphere and ocean in the tropical Pacific that results in somewhat (semi) periodic variations between below-normal and above-normal sea

surface temperatures (SSTs) and dry and wet conditions over the course of a few years [46], [47]. The El Niño and La Niña events occur typically over the interannual time scales, characterizing the processes of ocean–atmosphere interaction in the eastern and western tropical Pacific [48]. El Niño is manifested by unusually warm ocean temperatures along the equatorial Pacific, whereas La Niña is characterized by unusually cold ocean temperatures in this region. The El Niño and La Niña events occur on average every 2–7 years. Typically, El Niño occurs more frequently than La Niña. El Niño typically lasts 9–12 months. La Niña typically lasts 1–3 years. Both tend to develop during March–June, reach peak intensity during December–April, and then weaken during May–July. However, prolonged El Niño episodes have lasted 2 years and even as long as 3–4 years.

The Southern Oscillation Index (SOI) is a measure of large-scale fluctuations in air pressure occurring between the western and eastern tropical Pacific during the ENSO (i.e., the El Niño and La Niña episodes). The SOI is calculated from the monthly or seasonal fluctuations in air pressure differences between Tahiti and Darwin. A strongly and consistently positive SOI pattern (e.g., consistently above about +7 over a two-month period) is related to a high probability with abnormally cold ocean waters across the eastern tropical Pacific typical for the La Niña episodes. Conversely, a “deep” and consistently negative SOI pattern (less than about  $-7$  over a two-month period) is related to coincide with abnormally warm ocean waters across the eastern tropical Pacific typical for the El Niño episodes. However, it is important to remember that the pattern of relationship between SOI and precipitation (and temperature) anomalies can vary depending on a particular season and region. In this study, we assessed a possible link between the ENSO and SLCs in HK. We used the monthly SOI data since 1876 provided by the Australian Bureau of Meteorology

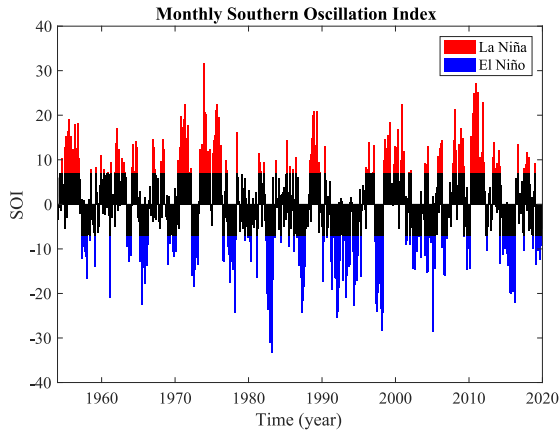


Fig. 4. Monthly SOI between 1954 and 2020.

(<http://www.bom.gov.au/climate/current/soi2.shtml>). They are multiplied by a factor 10 to make the SOI range from about  $-35$  to about  $+35$  and the value of the SOI can be quoted as a whole number. As mentioned above, the sustained negative values of the SOI lower than  $-7$  often indicate the El Niño episodes. The sustained positive values of the SOI greater than  $+7$  are typical for the La Niña episodes. The time series of monthly SOI between 1954 and 2020 is plotted in Fig. 4.

There are also many other ENSO indices, such as the Niño SST and the multivariate ENSO index (MEI) (<https://climatedataguide.ucar.edu/climate-data>). The Niño SST indices are derived from the SST anomalies in different areas of the equatorial Pacific, which include Niño 1+2 (0-10S, 90W-80W), Niño 3 (5N-5S, 150W-90W), Niño 3.4 (5N-5S, 170W-120W), Niño 4 (5N-5S, 160E-150W), and the oceanic Niño index. The MEI is calculated from a more holistic representation of the atmospheric and oceanic anomalies (such as sea-level pressure, zonal and meridional components of the surface wind, SST, and outgoing longwave radiation) that occur during the ENSO events. To investigate these events more rigorously, we compared different ENSO indices, namely SOI (based on sea air pressure), Niño 3.4 (based on SST), and MEI (based on six atmospheric and oceanic variables). The time series of these standardized ENSO indices between 1980 and 2020 is shown in Fig. 5. The SOI indices have a high negative correlation with the MEI indices ( $-0.81$ ) and Niño 3.4 ( $-0.69$ ), whereas the MEI and Niño 3.4 indices are positively correlated with their correlation up to  $0.79$ . In addition, the El Niño and La Niña events are also indicated. The El Niño and La Niña always alternate with a variable frequency and duration. Since 1980, the three very strong El Niño episodes occurred during 1982–1983, 1997–1998, and 2015–2016. There were also other El Niño events, which occurred during 1987–1988, 2002–2003, 2006–2007, and 2009–2010. Between 1980 and 2020, the La Niña events occurred in 1988–1989, 1998–2001, 2008–2009, 2010–2012, and 2017–2018.

### III. DATA PROCESSING STRATEGY

The data processing comprised the application of the ocean-tide and inverted barometer corrections. We then applied the

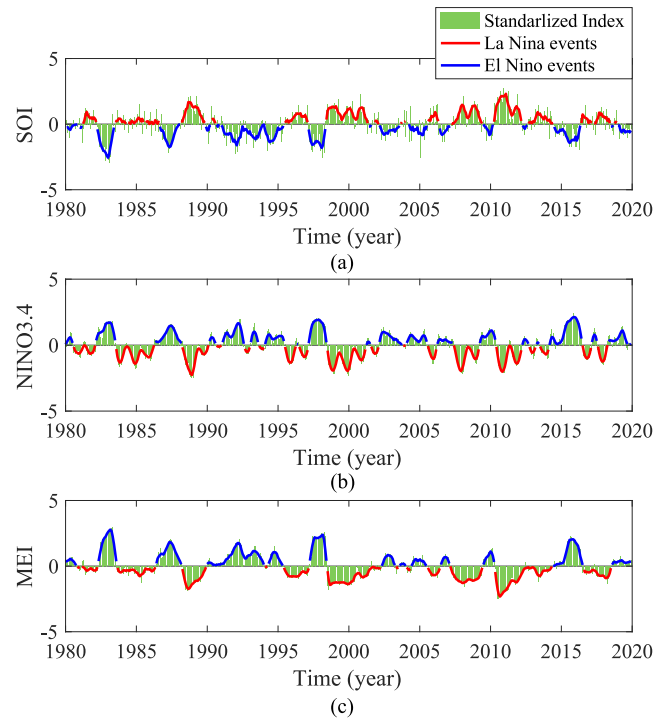


Fig. 5. Time series of three standardized ENSO indices: (a) SOI, (b) Niño 3.4, and (c) MEI during 1980–2020.

multiple regression and principal component analyses (PCAs) to investigate the corrected TG time series. These methods are briefly described as follows.

#### A. Harmonic Tidal Analysis

The ocean-tide effect can be removed by applying the harmonic analysis or by averaging TG records over a sufficiently long time period. In this study, we used the harmonic analysis to model and remove ocean-tide signal from TG data. The harmonic tidal analysis was applied to a time series at every TG station [49]. It produced 37 tidal constituents from low to high frequencies for every time series and was treated as the sum of the subtides of each cycle so that

$$\text{TG}(t) = a + bt + \sum_{i=1}^{37} A_i \sin\left(\frac{2\pi t}{P_i} + \varphi_i\right) + \varepsilon \quad (1)$$

where  $t$  is the time of the TG record, TG is the sea-level record observed from TG station at epoch  $t$ ,  $a$  and  $b$  are the constant and linear terms, respectively,  $A_i$  and  $\varphi_i$  denote the amplitudes and phases of each tidal constituent respectively, and  $P_i$  are the periods of each tidal constituent.

The amplitudes of 37 tidal components at each station were computed by applying the least squares analysis and then deducted from the TG records. In this way, the seasonal, interannual, and decadal signals as well as secular variations remained in the time series of tidal records.

### B. Inverted Barometer Effect Correction

The sea surface height change influenced by atmospheric pressure variations is described by a traditional inverted barometer equation [50]. It reads

$$IBe = -(P_{slm} - P_{ref}) / \rho g \quad (2)$$

where  $\rho$  is the seawater density,  $g$  is the gravity at the sea surface, and  $P_{slm}$  and  $P_{ref}$  are the local and global mean atmospheric pressure values, respectively.

We first computed the global monthly mean atmospheric pressure  $P_{ref}$  based on the global sea surface atmospheric pressure data from 1954 to 2019, as reanalyzed by NCEP/NCAR of NOAA.  $P_{slm}$  of each station was computed by applying a bilinear interpolation from the NCEP sea-level atmospheric pressure data. For midlatitudes, such as HK, we set  $\frac{1}{\rho g} = 9.948$  [51].

### C. Multiple Regression Analysis

After deducting the high-frequency ocean-tide signals by applying the harmonic tidal analysis, the seasonal, annual, and long-periodic terms can be observed in the monthly mean sea-level data in HK. In order to determine the long-term SLC rate while taking the interannual and long-periodic tidal terms into account, we applied a multiple regression analysis. We considered six periodic terms in the agreement with the procedure applied before by Ding *et al.* [29]. They took into consideration 18.6-year long-periodic signal, three interannual terms (with periods of 2, 4.94, and 7 years), and annual and semiannual terms. The long-term linear rate, the magnitudes, and phases of periodic signals in the SLCs were simultaneously estimated by a multiple regression model and based on applying the least squares analysis. The observation equation reads

$$SL(t) = a + bt + \sum_{i=1}^6 B_i \sin\left(\frac{2\pi t}{P_i} + \varphi_i\right) + \varepsilon \quad (3)$$

where  $t$  is the time (monthly),  $SL(t)$  are the monthly mean sea-level records observed at six TG stations at an epoch  $t$ ,  $a$  and  $b$  are constant and linear terms,  $B_i$  and  $\varphi_i$  are the amplitudes and phases of periodic signals, respectively, and  $P_i$  are the periods of each periodic signal (i.e.,  $P_i = 0.5, 1, 2, 4.94, 7.75, \text{ and } 18.6$  years).

### D. Empirical Orthogonal Functions

The EOFs, also known as a PCA, can be used to analyze the variance contribution of different components for extracting spatiotemporal features [52], [53]. The orthogonal basis is derived by computing the eigenvectors of a spatially weighted anomaly covariance matrix and the corresponding eigenvalues provide a measure of the percent variance explained by each pattern. Therefore, EOFs of a space-time physical process can be represented mutually by orthogonal space patterns where the data variance is concentrated with the first pattern being responsible for the largest part of the variance, the second for the largest part of the remaining variance, and so on. We then

TABLE II  
AMPLITUDE AND PHASE OF THE MAIN FIVE TIDAL CONSTITUENTS OF TG STATIONS IN HK

tides(days/cycle)		'M2'	'S2'	'N2'	'K1'	'O1'
		0.5175	0.5000	0.5274	0.9973	1.0758
QUB	Amp	39.29	15.59	8.34	35.48	28.48
	Phase	1.19	-1.11	-0.25	-1.22	1.04
TPK	Amp	35.68	14.23	7.62	34.92	28.15
	Phase	1.29	-1.04	-0.12	-1.11	1.13
WAG	Amp	35.50	14.05	7.69	34.64	27.88
	Phase	1.13	-1.18	-0.30	-1.22	1.02
TBT	Amp	58.82	21.72	11.46	39.08	30.55
	Phase	1.96	-0.21	0.53	-0.88	1.35
SPW	Amp	44.30	17.51	9.31	36.58	29.12
	Phase	1.30	-0.97	-0.14	-1.18	1.03
TMW	Amp	36.08	14.29	7.75	34.35	27.39
	Phase	1.13	-1.20	-0.30	-1.21	1.00

write

$$\mathbf{Y} = (y_1, y_2, \dots, y_m) = \begin{bmatrix} y_{11} & \dots & y_{1m} \\ y_{21} & \dots & y_{2m} \\ \vdots & \ddots & \vdots \\ y_{n1} & \dots & y_{nm} \end{bmatrix} \quad (4)$$

where  $n$  is the number of TG stations, and  $m$  denotes the number of a time period. In addition, the covariance matrix  $C$  of time series is orthogonally decomposed as follows:

$$C = \frac{1}{m} \mathbf{Y} \mathbf{Y}^T \quad (5)$$

$$C = \mathbf{E} \mathbf{\Lambda} \mathbf{E}^T = \begin{bmatrix} \lambda_1 & \dots & 0 \\ \vdots & \ddots & \vdots \\ 0 & \dots & \lambda_n \end{bmatrix} \begin{bmatrix} e_1^T \\ e_2^T \\ \vdots \\ e_n^T \end{bmatrix} \quad (6)$$

where  $\lambda_1 > \lambda_2 > \dots > \lambda_p$ . The orthogonal decomposition of the space domain can be computed as the feature vector of  $\mathbf{Y} \mathbf{Y}^T$ , and the EOF value can then be obtained by normalizing the decomposition. In addition, the PC  $Z$  can be calculated in the time series according to the following expressions:

$$\mathbf{EOF} = \mathbf{E} * \text{diag} \left( \frac{1}{\sqrt{\sum E^2}} \right) \quad (7)$$

$$\mathbf{Z} = \mathbf{E}^T \mathbf{Y}. \quad (8)$$

## IV. RESULTS

### A. Harmonic Tidal Analysis

To eliminate the impact of high-frequency ocean tides while focusing on the long-term SLCs, we analyzed the 37 known periods of tidal constituents and removed them from TG records. The amplitudes and phases of the main five tidal constituents of TG stations in HK are summarized in Table II. The largest amplitude is detected at the TBT station, followed by the SPW

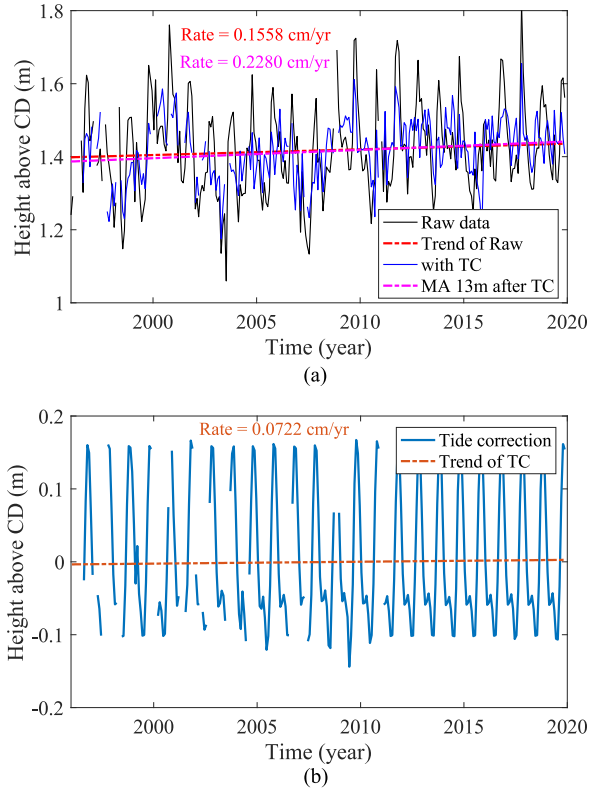


Fig. 6. (a) Monthly sea level at the QUB station before and after applying the ocean-tide correction. (b) Fitting the ocean tide at the QUB station.

station. Both TBT and SPW stations are located at the Pearl River Estuary. This finding is explained by the freshwater discharge and sedimentation at the estuary that are responsible for larger periodic fluctuations in sea-level trend at the western side of HK [24], [54]. On the other hand, the amplitudes of the main tidal components at the four stations at the eastern coast of HK are relatively consistent. The sea-level records at these stations are affected by oceanic currents from the east and storm surges due to typhoons as well as the northeast monsoon in winter [29], [55].

To investigate the effect of the high-frequency ocean tides on long-term SLCs (which has a low-frequency character), we compared the SLCs before and after applying the ocean-tide correction. As an example, the result for the TMW station is shown in Fig. 6. As seen, the ocean-tide correction contributed to a rate of 0.7 mm/yr of the SLC at a particular station between 1996 and 2019, resulting in an uncertainty of about 32% in the SLC rate (of 2.28 mm/yr).

### B. Inverted Barometer Effect

We used the monthly sea-level surface pressure data provided by the NCEP to correct the TG data for the inverse barometer pressure. As seen from the comparison of the sea-level rise rates estimated from the TG data before and after removing the inverted barometer effect, the results are quite consistent (see Fig. 7). This effect, for instance, at the QUB station is 0.45 mm/yr.

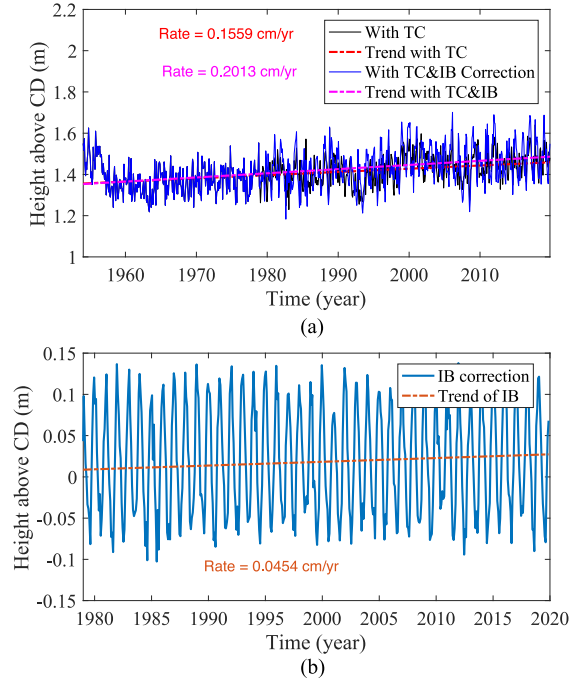


Fig. 7. (a) Time series and the trend of monthly sea level at the QUB station before and after applying the inverted barometer correction. (b) Time series and the trend of inverted barometer correction.

TABLE III  
SLC RATES ESTIMATED FROM RAW TG RECORDS AND AFTER APPLYING THE OCEAN-TIDE (TC) AND INVERTED BAROMETER CORRECTIONS (MM/YR)

	Time period	Raw	with TC	with TC and IB corrections
QUB	1954 - 2020	1.549±0.358	1.559±0.356	2.013±0.383
TPK	1997 - 2020	2.907±0.420	2.954±0.410	3.425±0.414
TBT	1994 - 2020	0.695±0.540	0.822±0.550	1.133±0.460
WAG	1963 - 2018	4.401±0.816	3.745±0.781	4.188±0.462
SPW	1974 - 2020	-	0.092±0.539	0.319±0.506
TMW	1976 - 2020	1.558±0.684	2.280±0.673	2.572±0.582

Rates of the SLC were estimated by applying the multivariable regression model, as described in (3). The SLC rates at six TG stations estimated from the raw TG records after applying the ocean-tide and inverted barometer corrections are shown in Fig. 8 and summarized in Table III. All the SLC rates passed the  $F$ -distribution test under the confidence level of 99%, with the  $p$ -value smaller than 0.01. The goodness-of-fit of the multivariate multivariable regression model of all stations ranges from 0.49 to 0.59. The effect of the ocean-tide correction on the SLC rate is between 0.1 and 0.8 mm/yr. The largest contribution on the estimated SLC rate is at the TMW station, where the difference of the SLC rate is up to 1.72 mm/yr, while at the sea-level rise rate, there is 2.57 mm/yr after applying the ocean-tide and inverse barometer corrections over the period from 1976 to 2020.

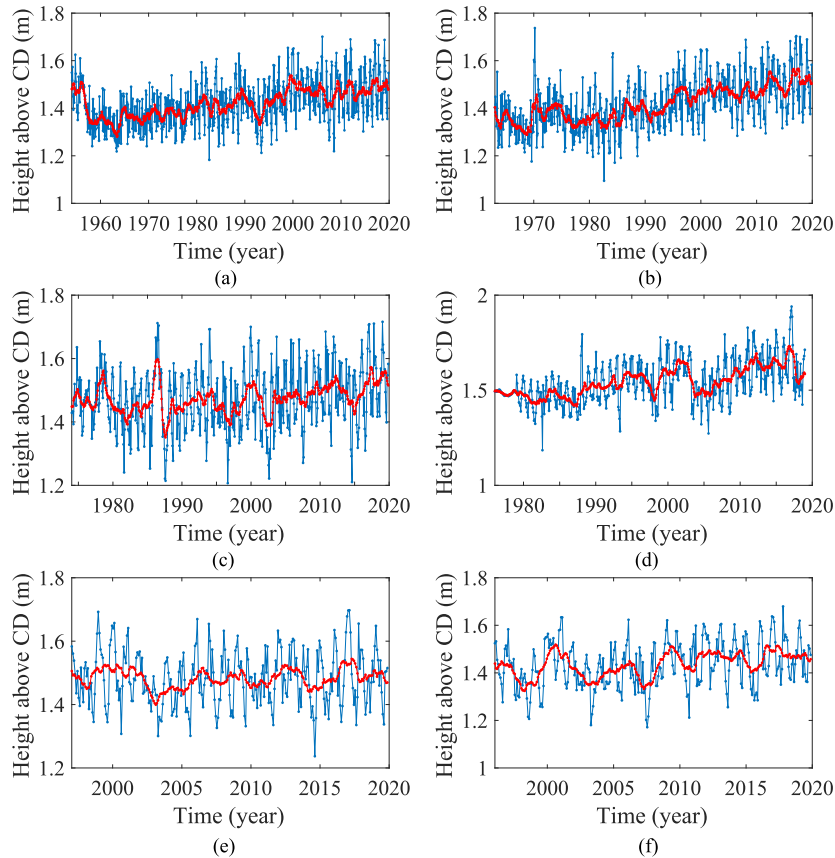


Fig. 8. (a) Time series and the 13-point moving averaging of monthly sea level at the TG stations. (a) QUB. (b) TPK. (c) TBT. (d) WAG. (e) SPW. (f) TMW.

From these findings, it is clear that the ocean-tide effect must be taken into consideration when estimating the rates of SLC from TG records (collected even for a few decades). The largest effect of the inverted barometer correction of 0.48 mm/yr was detected at the TPK station. It constitutes about 14% of the sea-level rise rate (3.43 mm/yr) at this station between 1997 and 2020.

After correcting for the ocean-tide and inverted barometer effects, we obtained the monthly mean SLCs. We also used a 13-point moving average to deduct changes with periods less than one year, including seasonal and annual changes. The results are presented in Fig. 8. We see an obvious increasing trend at all six stations. In order to compare the SLC rates measured by various stations over the same period, we computed the SLC rates at the six stations from 1997 to 2020. The results indicate that the relative sea-level rates at TG stations located in East HK, such as the WAG (5.08 mm/yr), TPK (4.00 mm/yr), and TMW (2.89 mm/yr) stations, are generally higher than those situated in West HK, just as TBT (3.06 mm/yr) and SPW (0.38 mm/yr). This is explained by the fact that TG stations in the eastern part are affected more directly by oceanic circulations in the SCS [56], [57].

### C. EOF Analysis

The analysis of spatiotemporal characteristics in TG records by applying the EOF analysis requires that these time series are continuous and consistent. For this reason, we used the monthly

mean sea-level data only over the period from 1997 to 2019. Before 1997, records at some TG stations were corrupted. We then applied the multiple regression analysis (3) to supplement the missing data. To analyze the spatiotemporal characteristics of SLCs, we first used a 13-point (13 months) moving average to deduct changes with periods less than one year, including seasonal and annual terms, given the fact that our interest is to estimate secular and interannual trends in the sea-level trend. We then applied the EOF method to the monthly mean SLCs.

Based on the monthly mean sea-level data from 1997 to 2019, the variance explained by the first three PCs accounts for 80.93% (see Table III) of six eigenvectors. This can reflect the main changes in sea-level trend at six TG stations in HK. The spatial eigenvectors of six eigen structures are summarized in Table IV. The corresponding time coefficients are shown in Fig. 9. Fig. 9(a) indicates that the overall trend of the temporal and spatial variations is positive, with the north stations having the largest positive values. In terms of time coefficients [i.e., Fig. 9(b)], there is an obvious upward trend from 1997 to 2019. Among them, time coefficients' changes kept relatively stable between 2003 and 2007. This indicates that the sea-level rise slowed down during this period. After 2007, the time coefficients' changes exhibit an accelerating trend. The sea level around HK follows this rule.

Fig. 8(c) and (d) shows the second eigenvector spatial distribution and corresponding time coefficient (the variance

TABLE IV  
EIGEN VALUES, VARIANCES, AND ACCUMULATIVE TOTAL VARIANCES OF DIFFERENT EIGEN STRUCTURES

PCs	PC 1	PC 2	PC 3	PC 4	PC 5	PC 6
<b>Eigen values</b>	3.41	0.80	0.63	0.55	0.38	0.22
<b>Variances (100%)</b>	57.12	13.34	10.47	9.16	6.31	3.60
<b>Accumulative variances (100%)</b>	57.12	70.46	80.93	90.09	96.40	100.00

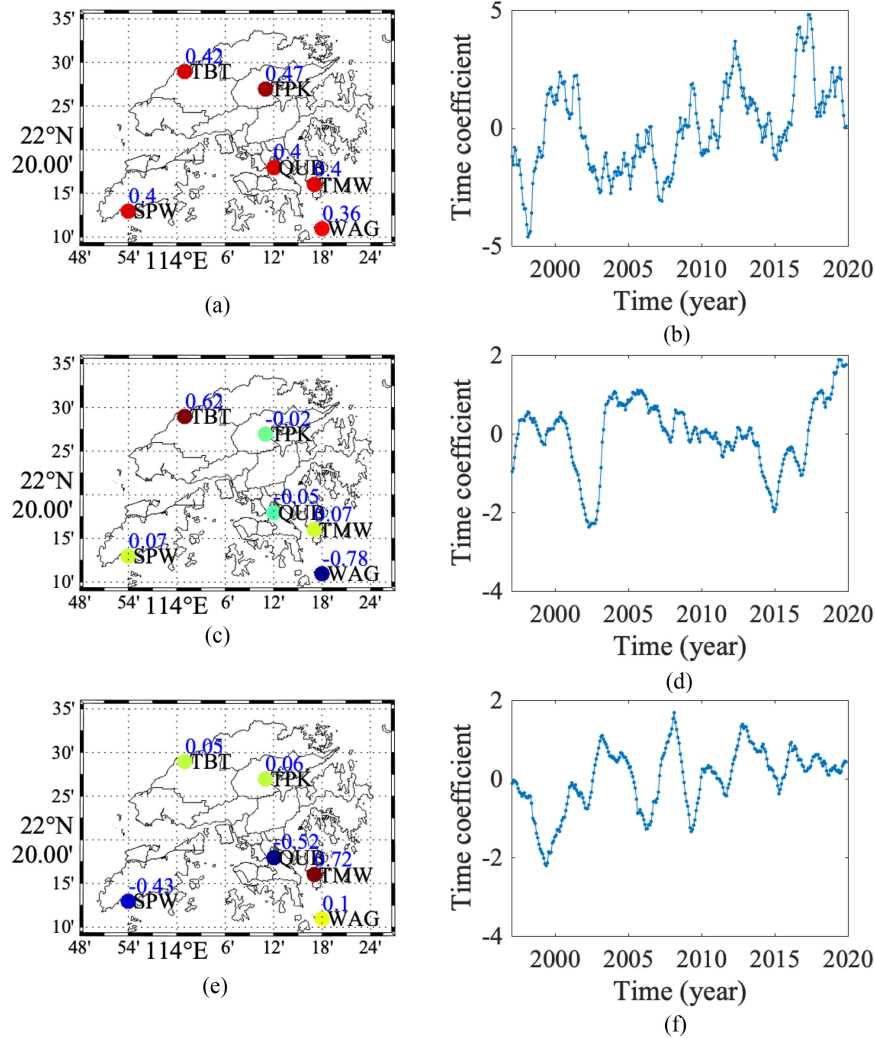


Fig. 9. First, second, and third EOFs of SLCS with their corresponding time coefficients at six TG stations in HK.

contribution value is 13.34%) derived from the EOF decomposition of sea-level trend in HK. Two obvious jumps can be found in 2003 and 2015 [see Fig. 9(d)]. A strongly positive trend was detected at the TBT station, while negative at the WAG station. This shows that the rate of sea-level rise at the TBT station dropped significantly in 2003 and 2015, while this decrease is much less obvious at other stations. Fig. 8(e) and (f) shows the third eigenvector spatial distribution and the corresponding time coefficient (the variance contribution value is 10.47%). We see strongly positive values at the TMW station, while significantly negative at the SPW and QUB stations.

TABLE V  
SPATIAL EIGENVECTORS FOR SIX TG STATIONS IN HK

	QUB	SPW	TBT	TMW	TPK	WAG
<b>PC 1</b>	0.40	0.40	0.42	0.47	0.40	0.36
<b>PC 2</b>	-0.05	0.07	0.62	-0.02	0.07	-0.78
<b>PC 3</b>	-0.52	-0.43	0.05	0.06	0.72	0.10
<b>PC 4</b>	0.66	-0.74	0.03	0.08	0.03	-0.08
<b>PC 5</b>	0.36	0.26	-0.19	-0.72	0.50	-0.09
<b>PC 6</b>	0.09	0.17	-0.64	0.51	0.24	-0.49

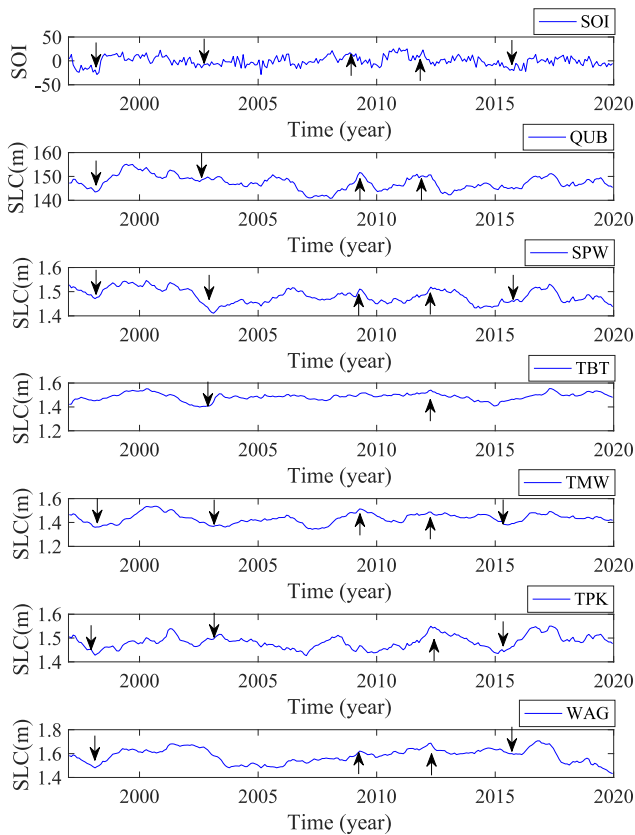


Fig. 10. Time series of monthly SOI and monthly SLCs at six TG stations in HK (QUB, SPW, TBT, TMW, TPK, and WAG).

#### D. Relative SLCs Versus ENSO

To analyze the relationship between the SLCs and the ENSO, we removed the long-term, annual, and semiannual changes from the monthly sea-level variations at six TG stations according to (2). In view of a high correlation between different ENSO indices, we selected the SOI index to analyze the impact of ENSO events on SLCs in HK. The time series of monthly SOI and monthly SLCs at six TG stations in HK between 1997 and 2020 is shown in Fig. 10. This comparison revealed that the SOI significantly controls SLCs in HK. Interannual sea-level fluctuations agree with the SOI changes. We see that in the presence of strong El Niño events in 1997–1998, 2002–2003, and 2015–2016, the SOI decreased and the sea level clearly dropped. During the La Niña events that followed the El Niño events in 2008–2009, 2011–2012, and 2017–2018, the SOI increased. This contributed to a rising sea level. We explain this by the location of HK in the West Pacific. When the La Niña events occur, the southeast trade wind blows the seawater heated by the sun to the West Pacific, causing the sea level to increase, while decrease in East Pacific. In contrast, during the strong El Niño events, the ocean water in the tropical Pacific flows eastward and rises the sea level in East Pacific. Currently, the sea level in West Pacific is lower than during a normal period.

We used the cross-correlation analysis to quantify the relationship between the occurrences of the La Niña and El Niño

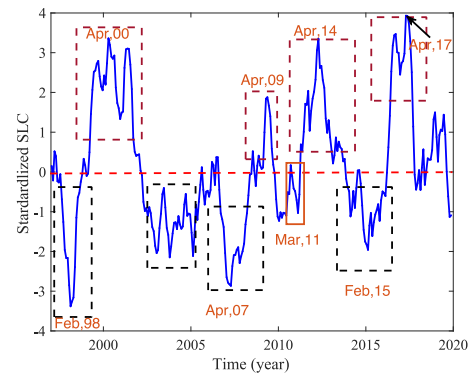


Fig. 11. Time series of interannual standardized SLCs in HK.

events and the interannual SLCs in HK. We found that the maximum positive correlation between the SOI and the SLCs is 0.42, and the SOI phase occurs eight months earlier than those of the interannual sea-level variations at the TMW station (at a 99% confidence level). The correlation between the SOI and the interannual SLCs at the other five stations is between 0.29 and 0.35, and the SOI phase occurs five months earlier than the phase of sea-level variations (at a 99% confidence level). These findings indicate the existence of several months time lag between the sea-level and SOI changes [41]–[43]. The SLCs in HK are clearly affected by the ocean–atmospheric interaction in the tropical Pacific associated with the El Niño and La Niña events.

Fig. 11 illustrates the SLC in HK calculated by applying the first PC estimation [see also Fig. 9(b)] of TG data at all six stations combined, which is the standardized SLC that indicates a regional general sea-level trend. We conducted a comparative study to investigate the relationship between the occurrences of La Niña/El Niño events and the interannual SLCs (after removing a secular trend). By comparing to the 13-month smoothed SOI, we find agreement between the sea-level and SOI variations during large ENSO events, although a high correlation coefficient does not exist between them (0.4 at a 99% confidence level). Contributed to the strong El Niño episodes, the sea level in HK in 1997–1998, 2002–2004, 2006–2007, and 2015–2016 was below the average from 1997 to 2019. During the strong La Niña episodes in 1998–2001, 2008–2009, and 2016–2017, the sea level in HK was above the average. This inverse relationship between the phases of ENSO and the annual cycle does imply a significant impact of ENSO on interannual sea-level fluctuation, with the El Niño reducing the amplitude of the annual cycle and the La Niña increasing the amplitude of the annual cycle.

Most tsunamis are caused by undersea earthquakes. Because of a geographical location of HK and the Philippines, the tsunami could not reach HK directly. Although tsunamis can be reached through refraction, their energy will greatly decline. Therefore, there is a little chance that HK will be affected by a serious tsunami. On March 11, 2011, a large tsunami occurred offshore of East Honshu in Japan that resulted in an SLC with the amplitude of about 20 cm. This earthquake-induced tsunami affected the sea level also in HK, as illustrated in Fig. 11. We

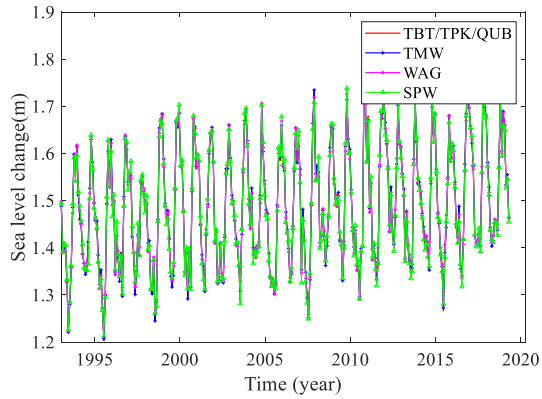


Fig. 12. Time series of the absolute SLCs from the nearest SA grid data to individual TG locations.

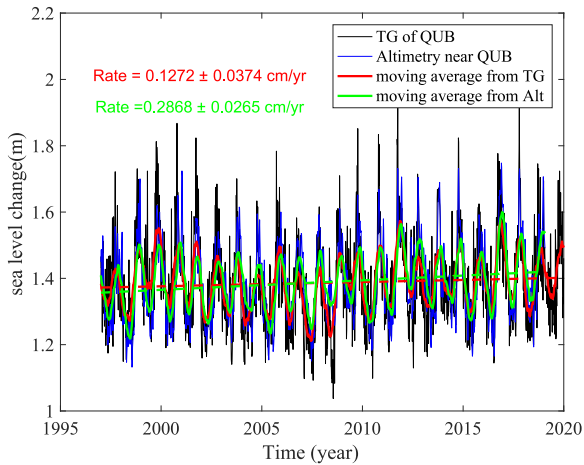


Fig. 13. Time series and moving average of SLCs from TG records at the QUB station (22.28°N, 114.22°E) and the grid altimetry measurements at a location of 22.25°N and 114.25°E.

see a sudden drop in the standard SLC between March 2011 and April 2011. The SLCs due to other tsunamis, such as those caused by December 2006 Taiwan earthquake or February 2010 Chile earthquake, were less than 10 cm and, thus, not apparent in the interannual standardized sea-level trend. We, therefore, argue that the ENSO is the most significant factor affecting the sea level in HK.

### E. Absolute SLCs

We used the AVISO monthly mean gridded sea-level anomalies between 1993 and 2019 to estimate the absolute SLC in HK. We tailored the nearest SA grid data to the individual TG locations. The absolute SLCs from the gridded SA data are summarized in Fig. 12. They show a high consistency at the rate of about 3.64–3.84 mm/yr from 1993 to 2019. The regional average of the SLC rate in HK is  $3.69 \pm 0.45$  mm/yr. In open oceans, the SLCs can be detected from the SA with a high precision, but their accuracy decreases dramatically near the coast [58], [59]. In this case, their comparison with the

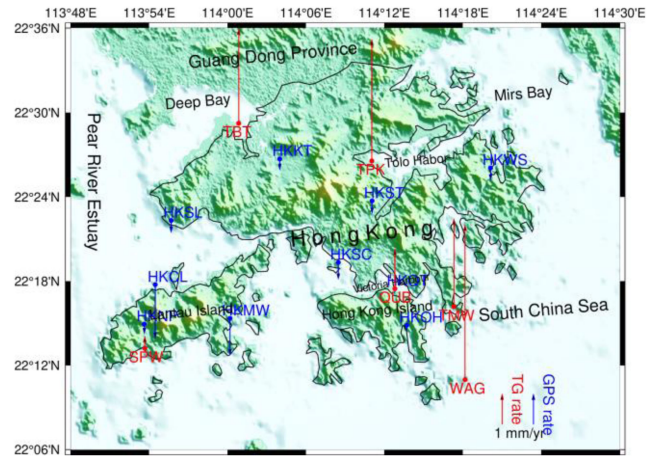


Fig. 14. SLC rates from TG records and the vertical displacement rate from GPS in HK.

corresponding estimates from the analysis of TG and GPS data is inevitable.

The example of the absolute and relative SLCs determined based on using SA and combined TG data at the QUB station is illustrated in Fig. 13. We see a consistent periodic signal of SLCs in both records. Usually, the amplitude of SLC recorded by the TG station is larger than that measured by SA due to a low resolution of SA. The SLC rate at the QUB station (22.28°N, 114.22°E) was only 1.27 mm/yr between 1997 and 2019, while the corresponding rate estimated by altimetry (22.25°N, 114.25°E) was 2.87 mm/yr over the same period. Moreover, these differences are obviously also attributed to vertical land motions. At the QUB station, this difference is about 1.6 mm/yr, and relatively similar differences were found at other stations (see Table V).

As stated above, the vertical land motion is an important factor that cannot be ignored when estimating the absolute SLC from TG records [55], [60]–[63]. In HK, these motions are mainly attributed to a subsidence due to the river delta sediment deposition, the construction of coastal high-rise buildings, and the excessive extraction of groundwater. We used the results of land vertical movement (measured at GPS stations situated near TG stations, which is provided by the SONEL of the GLOSS to estimate the absolute SLCs. The GPS stations with long-term records were selected to be located as close as possible to TGs (<10 km). The vertical land movements in HK are summarized, as shown in Fig. 14, and summarized in Table IV. The largest subsidence is detected at the Lantau Island at the HKCL ( $-1.77 \pm 1.15$  mm/yr) and HKMW ( $-1.21 \pm 0.72$  mm/yr) stations. The subsidence rates at the HKQT and HKOH sites at the HK Island are both  $-0.15$  mm/yr. The vertical displacement rates at GPS stations located in Kowloon and the New Territories are between 0.2 and 0.6 mm/yr.

There are two hypotheses necessary when using GPS data to correct vertical land movements in TG records (only for the long-term sea-level assessment and not for the altimeter calibration) [61]. In the first hypothesis, we assumed that the vertical land motion estimated from GPS data is consistent over the TG data period. Following this hypothesis, the vertical land

TABLE VI  
ABSOLUTE SLC RATES FROM THE ANALYSIS OF THE TG AND GPS (TG+GPS) AND SA DATA (UNIT: MM/YR)

TG station	Relative SLC rate	Nearby GPS Station	Land subsidence Rate	Absolute SLC rate from TG+GPS	Absolute SLC rate from SA
QUB	1.3±0.58	HKQT	-0.15±1.02	1.59	2.87
		HKOH	-0.15 ±0.63		
		HKSC	-0.56 ±0.62		
SPW	0.38±0.56	HKCL	-1.77 ±1.15	1.48	2.72
		HKMW	-1.21 ± 0.72		
		HKNP	-0.33±0.68		
TBT	3.06±0.63	HKSL	-0.4±0.61	3.44	2.87
		HKKT	-0.36±0.02		
TPK	4.00±0.68	HKST	-0.42±0.02	4.42	2.87
TMW	2.89±0.59	HKOH	-0.15 ±0.63	3.10	2.99
		HKWS	-0.26±0.04		
WAG	5.08±0.90	-	-	-	2.94

movements would be perfectly captured by a linear trend that would be then used to correct the relative sea-level trend. The second hypothesis requires that the land motion detected by GPS is representative of vertical ground motion at the TG station benchmark and the vertical land motion in adjacent areas is uniform. The estimated absolute SLC rates in HK from the analysis of TG and GPS data are summarized and compared with the corresponding estimates from the SA in Table VI. As seen, the absolute SLCs in Kowloon and the New Territories are about 3–4 mm/yr. The largest SLC is found in the WAG (5.23 mm/yr), but information about the vertical land motion on this island is not available. The HK Island has the smallest absolute SLC rate of only 1.59 mm/yr at the QUB station.

If estimates of the absolute SLCs from both methods are available, we recommend using the TG and GPS estimates at the QUB, TBT, SPW, TMW, and TPK sites because residual ocean signals might correlate over long distances that will pollute SA measurements. However, if large discrepancies ( $>3$  mm/yr) between the two methods exist, the local vertical land motion differences between the TG and near GPS station are likely incorrect. In this case, it is better to take the altimetric estimate. This is the case for the WAG site.

## V. DISCUSSION

Our estimates of the regional SLC rates ( $2.5 \pm 0.93$  mm/yr from TG records between 1997 and 2019, and  $3.69 \pm 0.45$  mm/yr from SA during 1993–2019) are consistent with previous studies [23], [24]. From 2000 to 2010, the sea-level rises in HK about  $3.10 \pm 0.19$  mm/yr when analyzing TG records. During the past decade from 2010 to 2019, the sea level in HK has been rising at an accelerating rate up to  $4.89 \pm 0.15$  mm/yr. This value is much higher than the global mean sea-level rate of 3.3 mm/yr during the past 27 years (see Fig. 15) [64], [65]. The reason

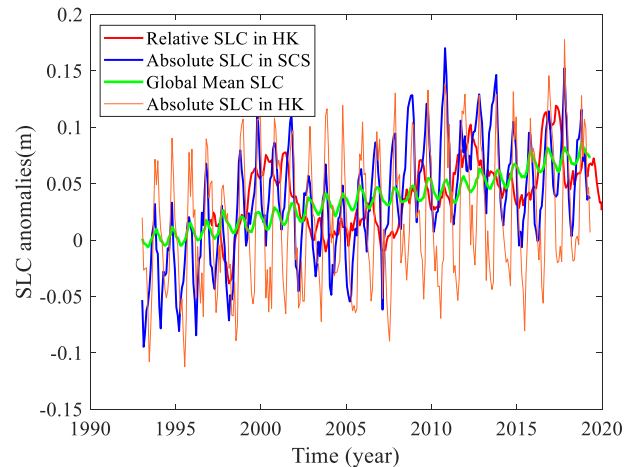


Fig. 15. Absolute sea-level anomalies from SA measurements and relative sea-level anomalies from TG records in the SCS, HK, and global mean SLC.

may be due to anomalous atmospheric and SST [41], [54], [58], [66]. Comparing the regional SLCs in HK with the SLCs in the SCS and global mean sea level indicates that the regional sea-level fluctuations in HK agreed well with SLCs in the SCS (see Fig. 15). The SLCs in the marine areas near HK are basically consistent with those in the SCS. We further investigated the impact of ENSO on temporal annual sea-level fluctuations. We found out that the sea level is below normal during the El Niño events, while above during the La Niña events. This finding agrees with the SA results and model outputs [36], [37], [41]–[43].

We find large uncertainties in GPS vertical land motion rates. Hen *et al.* (2010) analyzed GPS records at 12 sites acquired during 2006–2007 in HK. They detected the vertical uplift at

nine sites at the rate of between 0.65 and 2.23 mm/yr, and the subsidence at three GPS sites at the rate of between 0.12 and 0.57 mm/yr [67]. Hu *et al.* [31] estimated the vertical displacements in HK from the analysis of the CORS network. They found out that the vertical displacement rates were between  $-15$  and  $27$  mm/yr during 2010–2017 [31]. Such large differences between estimates of the vertical land motions in published studies might be explained by larger errors in vertical component as well as relatively small vertical land motions. We also found relatively large differences of about 1–2 mm/yr between the estimates of the absolute SLC rates from the analysis of the TG and GPS data in comparison with SA measurements. Uncertainties in GPS vertical displacement are one of the many reasons. Due to near coast effects, ocean-tide models introduce the biggest errors in decimeter level in the SA measurements [58]. If trend estimates from both the TG and GPS data and SA measurements are available, we recommend using the former. If large discrepancies ( $> 3$  mm/yr) between these two methods exist (or there are no nearby GPS stations), it is better to use the latter estimates.

## VI. SUMMARY

HK, which is under increasing pressure from population growth, climate change and expanding economic development face unique risks from storm surge events and sea-level rise. The understanding of the spatiotemporal pattern and mechanism of ocean circulation and SLC is, therefore, especially important. In this study, we addressed these issues by investigating the spatial and temporal distribution and possible factors of SLC in HK. We also estimated the absolute SLCs in HK from the TG and GPS data analysis and compared the results with the SA measurements.

We have analyzed the SLCs in HK using the TG records at six stations over the period between 1954 and 2019. We applied the ocean-tide and inverse barometer corrections to TG data. The results show that the impact of the ocean tide and atmospheric pressure on SLC estimates differs even within relatively small distances between TG stations in HK. The application of the ocean-tide and inverse barometer corrections must be done when processing TG records to analyze the long-term and interannual SLC. The ocean-tide correction resulting in uncertainties of about 32% in the measured SLC rate at the TMW station. The largest effect of the inverted barometer correction was detected at the TPK station and contributed about 14% of the SLC rate at TPK.

The estimated rates of relative SLC at six TG stations in HK after applying these two corrections were between 0.05 and 0.36 mm/yr over the period between 1954 and 2019. Our results reveal that the relative SLC rate is  $2.0 \pm 0.4$  mm/yr over the period of 65 years between 1954 and 2019. We also found out, based on the analysis of TG and GPS data, that the absolute SLC at the QUB site (located at the HK Island) was at the rate of 1.59 mm/yr between 2000 and 2019. Moreover, over the past decade (2010–2019), the sea-level rise has been accelerating at the rate up to 5.1 mm/yr. This value exceeds significantly the global mean sea-level rise at the rate of 3.3 mm/yr.

We applied the EOF method to study the temporal and spatial characteristics of SLCs in HK and analyzed the possible link between the SLCs and ENSO. The results (i.e., EOF1) confirmed that the sea-level rise trend between 1997 and 2020, with two interannual modifications of this secular trend in 2002–2003 and 2015–2016, was due to ENSO. The ENSO is the most significant factor affecting the SLCs in HK.

The analysis of the SA data revealed that the absolute SLC around HK is highly consistent at the rate of 3.69 mm/yr between 1993 and 2019. The analysis of GPS data in HK over the period between 1997 and 2019 revealed a prevailing land subsidence at different rates in different parts of the HK territories. The analysis of GPS and TG data (over the same period) indicates that the absolute SLC in Kowloon and New Territories is about 3 to 4 mm/yr, while only about 1.6 mm/yr at the HK Island. The absolute sea level estimated using SA measurements (again over the same period) is about 2.9 mm/yr. These results can serve as the basis for implementing appropriate measures to prevent the long-term impact of SLC in HK, particularly focusing on a reclamation land.

## ACKNOWLEDGMENT

The authors would like to thank the anonymous reviewers for their helpful comments, the Hong Kong Observatory for providing the tide gauge data, the Australian Bureau of Meteorology for providing SOI data, and the National Center for Atmospheric Research for providing the ENSO index and the SONEL of the global sea-level observing system for GNSS data.

*Author Contributions:* Fang Zou performed numerical studies and prepared a draft of the manuscript; Robert Tenzer coordinated this research and compiled the final version of the manuscript. Hok Sum Fok, Guojie Meng, and Qian Zhao revised the manuscript.

*Conflicts of Interest:* The authors declare no conflict of interest. The founding sponsors had no role in the design of the study; in the collection, analyses, or interpretation of data; in the writing of the manuscript; or in the decision to publish the results.

## REFERENCES

- [1] C. M. Duarte, "The future of seagrass meadows," *Environ. Conservation*, vol. 29, no. 2, pp. 192–206, 2002.
- [2] J. A. Church and N. J. White, "A 20th century acceleration in global sea-level rise," *Geophys. Res. Lett.*, vol. 33, no. 1, 2006, Art. no. L01602.
- [3] G. A. Meehl *et al.*, "How much more global warming and sea level rise," *Science*, vol. 307, no. 5716, pp. 1769–1772, 2005.
- [4] B. H. Strauss, "Rapid accumulation of committed sea-level rise from global warming," *Proc. Nat. Acad. Sci. United States Amer.*, vol. 110, no. 34, pp. 13699–13700, 2013.
- [5] S. Jin and F. Zou, "Re-estimation of glacier mass loss in Greenland from GRACE with correction of land–ocean leakage effects," *Global Planet. Change*, vol. 135, pp. 170–178, 2015.
- [6] F. Zou, R. Tenzer, H. S. Fok, and J. E. Nichol, "Mass balance of the Greenland ice sheet from GRACE and surface mass balance modelling," *Water*, vol. 12, no. 7, 2020, Art. no. 1847.
- [7] J. L. Chen, C. R. Wilson, and B. D. Tapley, "Contribution of ice sheet and mountain glacier melt to recent sea level rise," *Nature Geosci.*, vol. 6, no. 7, pp. 549–552, 2013.
- [8] T. Jacob, J. Wahr, W. T. Pfeffer, and S. Swenson, "Recent contributions of glaciers and ice caps to sea level rise," *Nature*, vol. 482, no. 7386, pp. 514–518, Feb. 2012.

- [9] E. Rignot, I. Velicogna, M. R. van den Broeke, A. Monaghan, and J. T. M. Lenaerts, "Acceleration of the contribution of the Greenland and Antarctic ice sheets to sea level rise," *Geophys. Res. Lett.*, vol. 38, no. 5, 2011, Art. no. L05503.
- [10] M. D. Palmer, G. R. Harris, and J. M. Gregory, "Extending CMIP5 projections of global mean temperature change and sea level rise due to thermal expansion using a physically-based emulator," *Environ. Res. Lett.*, vol. 13, no. 8, 2018, Art. no. 084003.
- [11] J. A. Church, J. S. Godfrey, D. R. Jackett, and T. J. Mcdougall, "A model of sea level rise caused by ocean thermal expansion," *J. Climate*, vol. 4, no. 4, pp. 438–456, 1991.
- [12] K. Lorbacher, M. Meinshausen, and A. Nauels, "Complementing thermocyclic sea level rise estimates," *Geosci. Model Develop.*, vol. 8, pp. 2723–2734, 2015.
- [13] R. K. Runting, C. E. Lovelock, H. L. Beyer, and J. R. Rhodes, "Costs and opportunities for preserving coastal wetlands under sea level rise," *Conservation Lett.*, vol. 10, no. 1, pp. 49–57, 2017.
- [14] L. Kuhfuss, H. Rey-Valette, E. Sourisseau, H. Heurtefeux, and X. Rufray, "Evaluating the impacts of sea level rise on coastal wetlands in Languedoc-Roussillon, France," *Environ. Sci. Policy*, vol. 59, pp. 26–34, 2016.
- [15] S. P. Leatherman, K. Zhang, and B. C. Douglas, "Sea level rise shown to drive coastal erosion," *Eos Trans. Amer. Geophys. Union*, vol. 81, no. 6, pp. 55–57, 2000.
- [16] J. Hinkel *et al.*, "A global analysis of erosion of sandy beaches and sea-level rise: An application of DIVA," *Global Planet. Change*, vol. 111, pp. 150–158, Dec. 2013.
- [17] T. L. Webster, D. L. Forbes, E. MacKinnon, and D. Roberts, "Flood-risk mapping for storm-surge events and sea-level rise using lidar for southeast New Brunswick," *Can. J. Remote Sens.*, vol. 32, no. 2, pp. 194–211, 2006.
- [18] M. Isobe, H. Mishima, and J. Tsutsui, "Prediction of flood due to storm surge under sea level rise in coastal area of Tokyo Bay," *Preprints Symp. Global Environ.*, vol. 2, pp. 168–173, 1994.
- [19] T. A. Watson, A. D. Werner, and C. T. Simmons, "Transience of seawater intrusion in response to sea level rise," *Water Resour. Res.*, vol. 46, no. 12, 2010, Art. no. W12533.
- [20] X. Collilieux and G. Wöppelmann, "Global sea-level rise and its relation to the terrestrial reference frame," *J. Geodesy*, vol. 85, no. 1, pp. 9–22, 2011.
- [21] V. Gornitz, "Sea-level rise: A review of recent past and near-future trends," *Earth Surf. Processes Landforms*, vol. 20, no. 1, pp. 7–20, Feb. 1995.
- [22] T. M. Cronin, "Rapid sea-level rise," *Quaternary Sci. Rev.*, vol. 56, pp. 11–30, Nov. 2012.
- [23] Y. Qu, Y. Liu, S. Jevrejeva, and L. P. Jackson, "Future sea level rise along the coast of China and adjacent region under 1.5 °C and 2.0 °C global warming," *Adv. Climate Change Res.*, vol. 11, no. 3, pp. 227–238, 2020.
- [24] B. Hong *et al.*, "Potential physical impacts of sea-level rise on the Pearl River Estuary, China," *J. Mar. Syst.*, vol. 201, 2020, Art. no. 103245.
- [25] B. Y. Lee, W. Wong, and W.-C. Woo, "Sea-level rise and storm surge—Impacts of climate change on Hong Kong," in *Proc. HKIE Civil Division Conf.*, 2010, pp. 1–6.
- [26] Y. Zhang, J. Xie, and L. Liu, "Investigating sea-level change and its impact on Hong Kong's coastal environment," *Ann. GIS*, vol. 17, no. 2, pp. 105–112, 2011.
- [27] Q. Yu, A. K. H. Lau, K. T. Tsang, and J. C. H. Fung, "Human damage assessments of coastal flooding for Hong Kong and the Pearl River Delta due to climate change-related sea level rise in the twenty-first century," *Natural Hazards*, vol. 92, pp. 1011–1038, 2018.
- [28] Y. Qu, S. Jevrejeva, L. P. Jackson, and J. C. Moore, "Coastal sea level rise around the China seas," *Global Planet. Change*, vol. 172, pp. 454–463, 2019.
- [29] X. Ding, D. Zheng, Y. Chen, J. Chao, and Z. Li, "Sea level change in Hong Kong from tide gauge measurements of 1954–1999," *J. Geodesy*, vol. 74, no. 10, pp. 683–689, 2001.
- [30] X. Ding, D. Zheng, W. T. Wong, K. W. Li, W. Chen, and P. Zhong, "Recent sea level variations in southern China from tide gauge observations," in *Proc. Asia-Pac. Space Geodyn. Symp.*, 2004, pp. 126–136.
- [31] B. Hu, J. Chen, and X. Zhang, "Monitoring the land subsidence area in a coastal urban area with InSAR and GNSS," *Sensors (Basel)*, vol. 19, no. 14, Jul. 2019, Art. no. 3181.
- [32] S. Qishi, L. Jiang, M. Jiang, H. Lin, P. Ma, and H. Wang, "Monitoring coastal reclamation subsidence in Hong Kong with distributed scatterer interferometry," *Remote Sens.*, vol. 10, no. 11, 2018, Art. no. 1738.
- [33] P. Ma *et al.*, "Remotely sensing large- and small-scale ground subsidence: A case study of the Guangdong–Hong Kong–Macao Greater Bay area of China," *Remote Sens. Environ.*, vol. 232, 2019, Art. no. 111282, doi: [10.1016/j.rse.2019.111282](https://doi.org/10.1016/j.rse.2019.111282).
- [34] H. B. Iz and C. K. Shum, "Mean sea level variation in the South China sea from four decades of tidal records in Hong Kong," *Mar. Geodesy*, vol. 23, no. 4, pp. 221–233, 2000.
- [35] H. Zhibo, G. Jinyun, T. Zhenguang, and C. Xiaotao, "Sea level variation in Hong Kong determined with Topex/Poseidon and tide gauge," *J. Geodesy Geodyn. (Chin.)*, vol. 34, no. 4, pp. 56–59, 2014.
- [36] W. T. Wong, K. W. Li, and K. H. Yeung, "Long term sea level change in Hong Kong," *Hong Kong Meteorol. Soc. Bull.*, vol. 13, pp. 24–40, 2003.
- [37] W. Wong and W.-C. Woo, "Sea-level change—Observations, causes and impacts," in *Proc. Hong Kong Inst. Eng. Conf. Climate Change – Hong Kong Eng. Persp.*, 2010.
- [38] C.-R. Ho, Q. Zheng, Y. S. Soong, N.-J. Kuo, and J.-H. Hu, "Seasonal variability of sea surface height in the South China sea observed with TOPEX/poseidon altimeter data," *J. Geophys. Res.*, vol. 105, no. C6, pp. 13981–13990, 2000.
- [39] C.-R. Wu and C.-W. J. Chang, "Interannual variability of the South China sea in a data assimilation model," *Geophys. Res. Lett.*, vol. 32, no. 17, 2005, Art. no. L17611.
- [40] X. Cheng, S.-P. Xie, Y. Du, J. Wang, X. Chen, and J. Wang, "Interannual-to-decadal variability and trends of sea level in the South China sea," *Climate Dyn.*, vol. 46, no. 9/10, pp. 3113–3126, 2016.
- [41] Y. Cheng, B. D. Hamlington, H.-P. Plag, and Q. Xu, "Influence of ENSO on the variation of annual sea level cycle in the South China sea," *Ocean Eng.*, vol. 126, pp. 343–352, 2016.
- [42] G. Han and W. Huang, "Low-frequency sea-level variability in the South China sea and its relationship to ENSO," *Theor. Appl. Climatol.*, vol. 97, no. 1/2, pp. 41–52, 2009.
- [43] Z. Rong, Y. Liu, H. Zong, and Y. Cheng, "Interannual sea level variability in the South China sea and its response to ENSO," *Global Planet. Change*, vol. 55, no. 4, pp. 257–272, 2007.
- [44] C. Wunsch and D. Stammer, "Atmospheric loading and the oceanic "inverted barometer" effect," *Rev. Geophys.*, vol. 35, no. 1, pp. 79–107, 1997.
- [45] D. B. Chelton and D. B. Enfield, "Ocean signals in tide gauge records," *J. Geophys. Res., Solid Earth*, vol. 91, no. B9, pp. 9081–9098, 1986.
- [46] H. S. Fok, Q. He, K. P. Chun, Z. Zhou, and T. Chu, "Application of ENSO and drought indices for water level reconstruction and prediction: A case study in the lower Mekong river estuary," *Water*, vol. 10, no. 1, 2018, Art. no. 58.
- [47] S. Ni, J. Chen, C. R. Wilson, J. Li, X. Hu, and R. Fu, "Global terrestrial water storage changes and connections to ENSO events," *Surv. Geophys.*, vol. 39, no. 1, pp. 1–22, 2018.
- [48] H. Zong, Y. Liu, P. Xiu, Q. Xu and Z. Rong, "Interannual variability of latent and sensible heat fluxes in the South China sea," *Chin. J. Oceanol. Limnol.*, vol. 28, no. 1, pp. 153–159, 2010.
- [49] M. Schwartz, *Encyclopedia of Coastal Science*. Amsterdam, The Netherlands: Springer, 2005.
- [50] S. R. Dickman, "Theoretical investigation of the oceanic inverted barometer response," *J. Geophys. Res., Solid Earth*, vol. 93, no. B12, pp. 14941–14946, 1988.
- [51] C. Wunsch, "Bermuda sea level in relation to times, weather, and baroclinic fluctuations," *Rev. Geophys. Space Phys.*, vol. 10, no. 1, pp. 1–49, 1972.
- [52] J. M. Wallace, "Empirical orthogonal representation of time series in the frequency domain—Part II: Application to the study of tropical wave disturbances," *J. Appl. Meteorol.*, vol. 11, no. 6, pp. 893–900, 1972.
- [53] G. R. Halliwell and J. S. Allen, "Large-scale sea level response to atmospheric forcing along the west coast of north america, summer 1973," *J. Phys. Oceanogr.*, vol. 14, no. 5, pp. 864–886, 1984.
- [54] W. Y. Wong, K. Y. Ma, L. M. Tsang, and K. H. Chu, "Genetic legacy of tertiary climatic change: A case study of two freshwater loaches, *Schistura fasciolata* and *Pseudogastromyzon Myersi*, in Hong Kong," *Heredity*, vol. 119, no. 5, pp. 360–370, Aug. 2017.
- [55] K. W. Li and H. Y. Mok, "Long term trends of the regional sea level changes in Hong Kong and the adjacent waters," in *Proc. 6th Int. Conf. Asian Pac. Coasts*, 2011, pp. 349–359.
- [56] Z. Huang, Y. Zong, and W. Zhang, "Coastal inundation due to sea level rise in the Pearl River Delta, China," *Natural Hazards*, vol. 33, no. 2, pp. 247–264, 2004.
- [57] S. Jilan, "Overview of the South China sea circulation and its influence on the coastal physical oceanography outside the Pearl River Estuary," *Continental Shelf Res.*, vol. 24, no. 16, pp. 1745–1760, 2004.
- [58] Y. Fu, X. Zhou, D. Zhou, W. Sun, and C. Jiang, "Sea level trend and variability in the South China sea," *ISPRS Ann. Photogramm., Remote Sens. Spatial Inf. Sci.*, vol. IV-2/W5, pp. 589–593, 2019.
- [59] A. Taqi, A. M. Al-Subhi, M. A. Alsaafani, and C. P. Abdulla, "Improving sea level anomaly precision from satellite altimetry using parameter correction in the Red sea," *Remote Sens.*, vol. 12, no. 5, 2020, Art. no. 764.

- [60] J. Wang, W. Gao, S. Xu, and L. Yu, "Evaluation of the combined risk of sea level rise, land subsidence, and storm surges on the coastal areas of Shanghai, China," *Climatic Change*, vol. 115, no. 3/4, pp. 537–558, 2012.
- [61] A. Santamaría-Gómez *et al.*, "Mitigating the effects of vertical land motion in tide gauge records using a state-of-the-art GPS velocity field," *Global Planet Change*, vol. 98–99, pp. 6–17, 2012.
- [62] A. Santamaría-Gómez, M. Gravelle, S. Dangendorf, M. Marcos, G. Spada, and G. Wöppelmann, "Uncertainty of the 20th century sea-level rise due to vertical land motion errors," *Earth Planet. Sci. Lett.*, vol. 473, pp. 24–32, 2017.
- [63] G. Wöppelmann and M. Marcos, "Vertical land motion as a key to understanding sea level change and variability," *Rev. Geophys.*, vol. 54, no. 1, pp. 64–92, 2016.
- [64] A. Cazenave, H.-B. Dieng, B. Meyssignac, K. von Schuckmann, B. Decharme, and E. Berthier, "The rate of sea-level rise," *Nature Climate Change*, vol. 4, no. 5, pp. 358–361, 2014.
- [65] J. A. Church and N. J. White, "Sea-level rise from the late 19th to the early 21st century," *Surv. Geophys.*, vol. 32, no. 4, pp. 585–602, 2011.
- [66] J. Chen, X. Wang, W. Zhou, and Z. Wen, "Interdecadal change in the summer SST-precipitation relationship around the late 1990s over the South China sea," *Climate Dyn.*, vol. 51, no. 5/6, pp. 2229–2246, 2018.
- [67] Q. Chen *et al.*, "Tight integration of GPS observations and persistent scatterer InSAR for detecting vertical ground motion in Hong Kong," *Int. J. Appl. Earth Observ. Geoinf.*, vol. 12, no. 6, pp. 477–486, 2010.



**Fang Zou** received the Dr. Phil. degree in astrometry and celestial mechanics from Shanghai Astronomical Observatory, Chinese Academy of Sciences, Shanghai, China, in 2018.

She is currently an Associate Research Professor with the Institute of Earthquake Forecasting, China Earthquake Administration, Beijing, China. Her research interests include global climate change, surface loading changes, and crustal deformations.



**Robert Tenzer** received the M.Sc. degree in geodesy and cartography and the Ph.D. degree in physical geodesy from Slovak Technical University, Bratislava, Slovakia, in 1995 and 1999, respectively, and the Ph.D. degree in satellite geodesy from Czech Technical University, Prague, Czech Republic, in 2008.

He is an Associate Professor with the Department of Land Surveying and Geo-Informatics, Hong Kong Polytechnic University, Hong Kong. From 2001 to 2008, he held research positions with the University of

New Brunswick, the University of Newcastle upon Tyne, and the Delft University of Technology; from 2009 to 2012, taught the University of Otago; and from 2012 to 2016, a Visiting Professor with the School of Geodesy and Geomatics, Wuhan University. His research interests cover broad areas of geodesy, geophysics, geodynamic, and planetary science, with a major focus on geospatial modeling techniques and interpretations, theoretical geodesy and geophysics, georeferencing, planetary inner structure, and processes. He is the author of 4 books and more than 200 research journal articles (184 records on Scopus and 177 records on WoS). He presented his research in more than 200 conference contributions and 60 invited lectures at universities around the world. He is the member of editorial board and Scientific Adviser to several journals while also contributing as the reviewer to more than 40 journals (including *Nature Geoscience*). He is currently the Chair of the Inter-Commission Committee on Theory joint study group JSG T.25: Combining geodetic and geophysical information for probing Earth's inner structure and its dynamics.



**Hok Sum Fok** received the B.S. and M.S. degrees in geomatics from Hong Kong Polytechnic University, Hong Kong, in 2003 and 2007, respectively, and the Ph.D. degree in geodetic science from Ohio State University, Columbus, OH, USA, in 2012.

From 2012 to 2013, he was a Postdoctoral Researcher with the School of Earth Sciences, Ohio State University. He is currently an Associate Professor with the School of Geodesy and Geomatics, Wuhan University, Wuhan, China.



**Guojie Meng** received the Ph.D. degree in geophysics from the Institute of Geophysics, China Earthquake Administration (CEA), Beijing, China, in 2002.

He is currently a Research Professor with the Institute of Earthquake Forecasting, CEA, Beijing, China. His research interests include GNSS data processing, earthquake deformation cycle, and earthquake hazard assessment.



**Qian Zhao** received the Ph.D. degree in geodesy and survey engineering from Wuhan University, Hubei, China, in 2012. Now she is an Associate Researcher with the Institute of Earthquake Forecasting, China Earthquake Administration, Beijing, China. Her research focuses on the satellite geodesy and geodynamic.